The Cryosphere Discuss., https://doi.org/10.5194/tc-2018-257
Manuscript under review for journal The Cryosphere
Discussion started: 6 December 2018

The Cryosphere Discussions
Open Access
EGU

Regional Grid Refinement in an Earth System Model: Impacts on the Simulated Greenland Surface Mass Balance

Leonardus van Kampenhout[1], Alan M. Rhoades[2], Adam R. Herrington[3], Colin M. Zarzycki[4], Jan T.M. Lenaerts[5], William J. Sacks[4], and Michiel R. van den Broeke[1]

[1]Institute for Marine and Atmospheric Research Utrecht, Utrecht University, The Netherlands
[2]Lawrence Berkeley National Laboratory, Berkeley CA, USA
[3]Stony Brook University, Stony Brook NY, USA
[4]National Center for Atmospheric Research, Boulder CO, USA
[5]Department of Atmospheric and Oceanic Sciences, University of Colorado, Boulder CO, USA

Correspondence: Leo van Kampenhout (L.vankampenhout@uu.nl)

Abstract. In this study, the resolution dependence of the simulated Greenland Ice Sheet surface mass balance in the variable-resolution Community Earth System Model (VR-CESM) is investigated. Coupled atmosphere-land simulations are performed on three regionally refined grids over Greenland at 1° (∼111 km), 0.5°(∼55 km), and 0.25° (∼28 km), maintaining a quasi-uniform resolution of 1°(∼111 km) over the rest of the globe. The SMB in the accumulation zone is significantly improved compared to airborne radar and in-situ observations, with a general wetting at the margins and a drying in the interior GrIS. Total precipitation decreases with resolution, which is in line with best-available regional climate model results. In the ablation zone, VR-CESM starts developing a positive SMB bias in some locations. Potential driving mechanisms are proposed, amongst which are diversions in large scale circulation, changes in cloud cover, and changes in summer snowfall. Overall, our results demonstrate that VR-CESM is a viable new tool in the cryospheric sciences and can be used to dynamically downscale future scenarios and/or be interactively coupled to dynamical ice sheet models.

1 Introduction

The relative contribution of the Greenland Ice Sheet (GrIS) to global sea level rise is increasingly determined through its surface mass balance (SMB) (van den Broeke et al., 2016). Accurate estimates of future GrIS SMB are therefore key in providing projections for sea level rise. Arguably the most realistic SMB projections to date are derived from general circulation model (GCM) scenario output downscaled using regional climate models (RCMs — e.g., Rae et al. (2012); van Angelen et al. (2013); Fettweis et al. (2013a); Mottram et al. (2017); Noël et al. (2018)). Compared to GCMs, the regional models offer more sophisticated snow models that have improved representation of albedo, melt, firn densification and refreezing, features that are lacking in most current GCMs (Ziemen et al., 2014; Helsen et al., 2017). In addition, RCMs typically run at a horizontal

grid resolution of $\mathcal{O}$(10 km) whereas atmospheric GCMs are typically run using 1° or $\mathcal{O}$(100 km) grids. RCMs therefore tend to better resolve topographic gradients which lead to more accurate spatio-temporal distributions in precipitation, wind, cloud cover, and temperature, enabling a detailed comparison to in-situ meteorological data. A fine spatial resolution seems indispensable for resolving narrow ablation zones found around the GrIS margins (Lefebre et al., 2005; Pollard, 2010).

Recently, significant efforts have been invested into making GCMs more suitable for ice sheet SMB modelling (e.g., Punge et al., 2012; Cullather et al., 2014; Fischer et al., 2014; van Kampenhout et al., 2017). In particular, improvements to the Community Earth System Model (CESM) include a multilayer snow model with a two-way radiative transfer model for albedo (Flanner and Zender, 2005), improved snow density parameterizations (van Kampenhout et al., 2017), and multiple elevation classes for downscaling SMB with height (Lipscomb et al., 2013).

Although globally uniform high-resolution climate simulations exist (50 km, Delworth et al. (2011); 25 km, Wehner et al. (2014); Small et al. (2014); 80 km, Müller et al. (2018)), a majority of ongoing modelling experiments, notably the forthcoming CMIP6 experiments (Eyring et al., 2016), maintain a ∼1° atmosphere grid due to limitations in computational resources. A middle road may be found in new techniques that apply regional grid refinement within a global climate model. In this approach, a static global mesh is constructed which has increased resolution over a specified region of interest. Over the past five years, rapid progress has been made in developing regional grid refinement in CESM — variable resolution or VR-CESM. Studies have been carried out looking at the effect of grid refinement on the global circulation and climatology (Zarzycki et al., 2015), the effect on tropical cyclones (Zarzycki and Jablonowski, 2014), regional climate in the presence of mountains (Rhoades et al., 2017; Huang et al., 2016; Rhoades et al., 2015), and the scale dependence of the underlying physics (Gettelman et al., 2018; Herrington and Reed, 2018). Compared to RCM downscaling, Huang et al. (2016) notes several advantages of the variable resolution (VR) approach. First, using a unified modelling framework avoids the inconsistencies between RCM and GCM, in particular the different dynamical core and physics that are used. Second, VR allows for two-way interactions (i.e., downstream / upstream feedbacks) between the refinement region and the global domain, which an RCM downscaling approach does not. Some more practical advantages are the relative simplicity of operating a single model and the relatively low computational cost associated with VR compared to a multi-model setup.

In this study, we apply VR-CESM over Greenland and evaluate the impact on GrIS SMB. In particular, we aim to understand the dependence of resolution on outstanding GrIS climate biases in CESM. Simulations are carried out at different spatial resolutions (i.e., 111, 55, and 28 km) over the greater Greenland region. Results are compared to airborne snow accumulation radar, in-situ SMB measurements, and gridded climate data from an RCM in an ongoing effort to improve the representation of ice sheets in CESM (Lipscomb et al., 2013; Vizcaíno et al., 2013; Lenaerts et al., 2016; van Kampenhout et al., 2017). A more in-depth evaluation of CESM over the GrIS, including surface energy balance, is planned for the upcoming release of CESM 2.1.

The layout of the manuscript is as follows. In Section 2, the modelling setup and benchmark data are described. Main results are presented in Section 3. The discussion in Section 4 is concerned with attributing the changes in ablation found across the different resolutions. Some general limitations of our modelling study are reviewed in Section 5. Finally, an overall summary as well as conclusions are provided in Section 6.

The Cryosphere Discuss., https://doi.org/10.5194/tc-2018-257
Manuscript under review for journal The Cryosphere
Discussion started: 6 December 2018

2 Methodology

2.1 Model description

The Community Earth System Model (CESM) is a global climate modelling framework comprised of several components, e.g. atmosphere, ocean, land surface, sea ice, and land ice, that may operate partially or fully coupled. When partially coupled, the missing components can be substituted by external data or even inactive (stub) components. Here, we follow the protocol of the Atmospheric Model Intercomparison Project (AMIP, Gates et al. (1999)) and dynamically couple the atmosphere-land components and prescribe ocean and sea ice data at monthly intervals. The prescribed sea ice and sea surface temperatures are taken from Hurrell et al. (2008) for the years of simulation 1980-1999. Aerosol and trace gas emissions are taken as observed.

2.1.1 Atmosphere model

The atmosphere component used is the Community Atmosphere Model (CAM) version 5.4 (Neale et al., 2012) with the spectral element (SE) dynamical core (Dennis et al., 2012; Lauritzen et al., 2018), the only dynamical core currently in CESM supporting VR capabilities (Zarzycki et al., 2014). Our model configuration is almost identical to that of Zarzycki and Jablonowski (2014), with a few small differences. These include updated rain and snowfall microphysics (MG2, Gettelman and Morrison (2014)), a new dry-mass vertical coordinate and slightly reduce horizontal diffusion in the SE dynamical core (Lauritzen et al., 2018), and the use of the Beljaars et al. (2004) orographic drag parameterization, replacing the turbulent mountain stress (TMS) scheme of CESM1 (Neale et al., 2012) in order to achieve higher and more realistic wind speeds over the ice sheets.

Hyperviscosity coefficients are to be scaled by the grid-resolution for numerical stability and filter undesirable numerical artifacts. In VR-CESM, local hyperviscosity coefficients are scaled by the underlying local element dimensions (Guba et al., 2014). Here the scaling is such that the hyperviscosity coefficients are reduced by an order of magnitude for each doubling of the resolution (Zarzycki and Jablonowski, 2014).

Note that whereas CAM-SE is an integral part of the release of CESM2, the VR framework is not yet officially supported. It is expected that a few scientifically validated VR-CESM simulations will be publicly available at a later stage during the release cycle of CESM2.

2.1.2 Land surface model

CAM is coupled to the Community Land Model (CLM) version 5.0, which incorporates several important bug fixes and snow parameters updates for CESM2. CLM simulates the interaction of the atmosphere with the land surface, notably the surface energy balance and hydrological processes such as interception by canopy, throughfall, infiltration, and runoff (Oleson, 2013). For radiation calculations over snow, the two-way radiative transfer model SNICAR is used (Flanner and Zender, 2005). The snow pack hydrological and thermal evolution is modelled as a one-dimensional column, which can reach depths of up to 10 metres of w.e. (water-equivalent). Several snow model modifications have been implemented specifically for ice sheets, such as wind-dependent fresh snow density and wind driven snow compaction (van Kampenhout et al., 2017) and temperature

The Cryosphere Discuss., https://doi.org/10.5194/tc-2018-257
Manuscript under review for journal The Cryosphere
Discussion started: 6 December 2018

dependent fresh snow grain size. Bare ice albedo is assumed constant, and is set to 0.50 (0.30) for the visible (near-infrared) spectrum, reflecting the distinction made between these two shortwave bands in CLM (Oleson, 2013).

Over glaciated grid cells, CLM maintains 10 different elevation classes in order to more accurately downscale SMB and temperature to the 4 km ice sheet grid with class weights proportional to the subgrid topography present in the grid cell (Lipscomb et al., 2013). Classes with zero weights are considered "virtual" and do not contribute to the grid cell average. In each elevation class or bin, CLM maintains a independent column for snow and ice (or soil, over tundra). These columns tend to evolve differently depending on their height, as temperature, specific humidity and longwave radiation are downscaled with elevation. Lapse rates are used for temperature (6 K km^{-1}) and longwave radiation (32 W m^{-2} km^{-1}), whereas specific humidity follows the assumption that relative humidity remains constant with height. Elevation classes have been shown to improve SMB gradients over Greenland (Vizcaíno et al., 2013). In order to activate elevation classes over Greenland, the Community Ice Sheet Model (CISM) must be active as a diagnostic component.

SMB is the main focus of this paper. We deviate from the standard CLM definition of SMB, which does not take into account changes in snow pack height, in favour of the definition that is common to glaciology, in absence of redistribution/erosion by drifting snow

$$\mathrm{SMB} = \mathrm{Precipitation} - \mathrm{Sublimation} - \mathrm{Runoff}. \quad (1)$$

For the remainder of the paper, modelled accumulation (ablation) is defined as modelled SMB for locations where SMB > 0 (SMB < 0). Unless indicated otherwise, annual CESM SMB data used have been downscaled to the 4 km CISM ice sheet grid, thus taking advantage of the multiple elevation classes in CLM. In this downscaling procedure, elevation classes are used in the vertical direction whereas a bi-linear interpolation is applied in the horizontal direction to prevent artificial jumps between grid cells (Leguy et al., 2018).

Following Rhoades et al. (2018), the distribution of plant functional types in CLM is assumed constant at year 2000 values for all simulations. As the main focus of this work is on precipitation and snow cover in non-vegetated regions, we argue this assumption has a negligible impact on our results.

2.1.3 Grids, time stepping, topography

Three identical atmosphere-land simulations are performed, each at a different grid. The first mesh is a standard, globally quasi-uniform grid at 1° (∼111 km) resolution. The simulation on this grid is referred to as Uniform CESM. The second mesh is nonuniform and has a refined patch of 0.5° (∼55 km) over the greater Greenland region, constructed using SQuadGen (Ullrich, 2014), and is referred to in this paper as VR-CESM55. The patch was constructed such that the boundary of the patch always extends at least six (nominally, $20\Delta x$) spectral elements away from the Greenland coast (Figure 1). This buffer region is intended to allow incoming "low-resolution" storms to develop finer-scale structures after entering the VR zone, and prior to making landfall. The third mesh is constructed from the VR-CESM55 grid but features a second level of refinement at 0.25° (∼28 km) inside the first level. Again, this second patch was chosen such that the boundary extends at least six spectral elements away from the Greenland coast. The simulation on this grid is referred to as VR-CESM28.

The Cryosphere Discuss., https://doi.org/10.5194/tc-2018-257
Manuscript under review for journal The Cryosphere
Discussion started: 6 December 2018

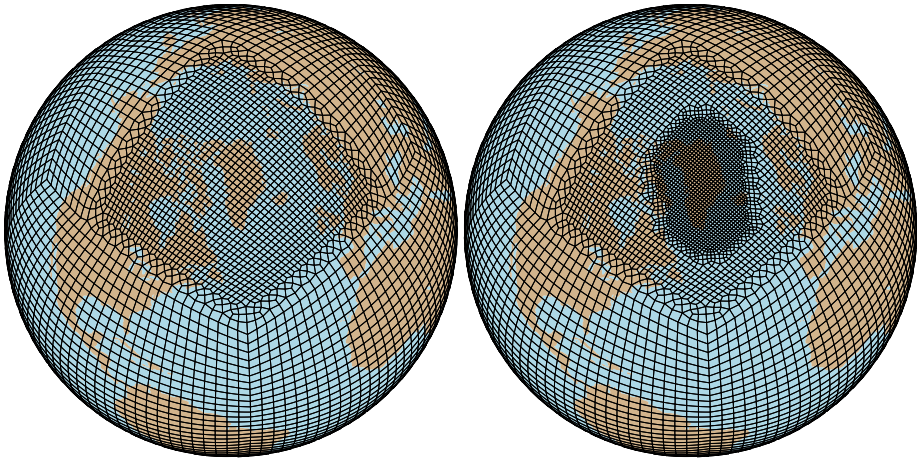

Figure 1. Computational domains of experiments VR-CESM55 (left) and VR-CESM28 (right). Each spectral element visible here contains an additional 3-by-3 grid of points, the exact position of which are determined by the spectral element method (Zarzycki and Jablonowski, 2014).

Topographic height over Greenland was interpolated from the 4 km CISM ice sheet domain, which in turn has been derived from the 90 m Greenland Ice Mapping Project product (GIMP, Howat et al. (2014)). Topography is static in time – ice sheet dynamics are not active in this configuration – a reasonable assumption for the decadal length simulations presented in this paper. The new ice topography was spliced into the global topography, similar to what is done in two-way coupled setups where ice sheet dynamics are turned on. Due to the hybrid sigma vertical coordinate system implemented in CAM-SE a differential smoothing procedure was applied to ensure numerical stability and realistic flow, as described in Zarzycki et al. (2015). Subgrid height variances, used by the orographic drag parameterization are consistently computed as a residual of the smoothed topography.

The resulting topographies are shown in Figure 2, with a rendering of GIMP for comparison. As one would expect, a more detailed and accurate representation of topography is possible on finer resolutions. The feature most prominently improving is the southern ice dome, that "rises up" from ∼2300 m at 111 km to ∼2900 m at 28 km. Furthermore, the 28 km resolution is sufficient to start resolving some of the fjord structures, especially in the east. The non-zero topographic heights over open ocean in Figure 2 are explained by the differential smoothing procedure.

The CAM physics (dynamics) time steps for Uniform CESM was 1800 (150) seconds. For the VR-CESM runs, the physics time step was set to 450 s and the CAM dynamics time steps scaled with horizontal resolution with VR-CESM55 at 150 s and VR-CESM28 at 75 s.

2.1.4 Initialisation

In glaciated regions, the subsurface conductive heat flux at the ice sheet surface is potentially large due to the high thermal conductivity of ice. To avoid unrealistic energy losses or gains from the subsurface, one should start with ice that is in thermal

The Cryosphere Discuss., https://doi.org/10.5194/tc-2018-257
Manuscript under review for journal The Cryosphere
Discussion started: 6 December 2018

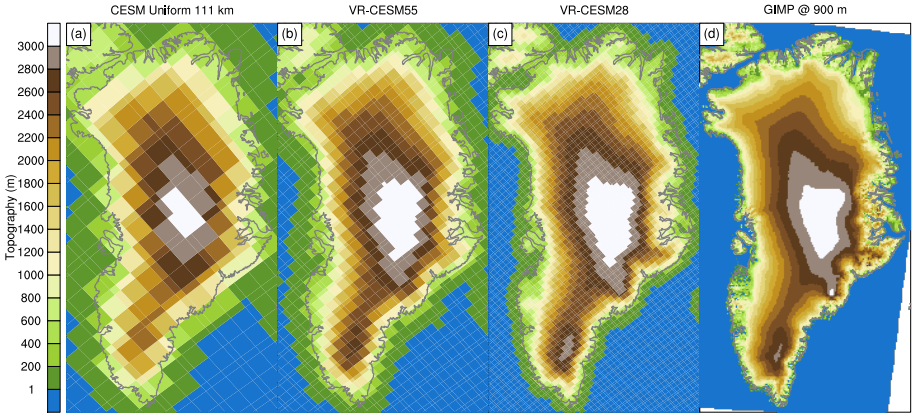

Figure 2. Topographic height in the three CESM simulations. For plotting purposes, spectral element node heights are displayed on control volumes equal to the area that they represent. The control volumes are identical to those used by the CESM coupler to conserve mass and energy. For reference, topographic height according to the Greenland Ice Mapping Project (GIMP, Howat et al. (2014)) is shown, which has been upscaled to 900 m.

equilibrium with the ambient climate. In our modelling setup, however, a sufficiently long spinup period to achieve such equilibrium was not feasible due to computational constraints. Instead, it was decided to initialise deep ice temperature from values close to observed, in this case 10 m firn temperatures from a firn densification model, forced by RCM-downscaled reanalysis data (Ligtenberg et al., 2018). A nearest neighbour procedure was followed to interpolate from the 11 km firn model to the different resolutions used in this study.

Snow height was reset globally to a low value of 100 mm w.e. to avoid snow cover hysteresis arising from errors in the interpolated initial conditions. This reset was limited to grid cells — or rather , CLM columns — below 1774 m, which is an estimate of the maximum present-day GrIS equilibrium line altitude. A spinup simulation was carried out to rebuild snow in any CLM columns residing below the reset altitude (1774 m) where the local climate dictates perennial snow cover. The relevance of this spinup is two-fold: (1) the dependence of fractional snow cover on snow height (Swenson and Lawrence, 2012), (2) the refreezing capacity of the snow pack. For both of these, a period of 5 years was deemed sufficiently long to capture the first-order effect. Nonetheless, it is recognised that the resulting snow depth distribution over the GrIS contains an artificial jump at 1774 m.

2.1.5 Performance

All simulations have been performed on NCAR's supercomputing facility "Cheyenne" in Wyoming, USA, which is equipped with Intel Broadwell processors. No real load-balancing was needed since the active components (i.e., CAM, CLM, CISM, coupler) perform well when sharing all the available cores. On 1800 cores (or 50 compute nodes) the cost of Uniform CESM at 1 ° amounts to ∼1070 core hours per simulated year. Keeping the number of cores the same, this cost was tripled to 3250 core hours for the VR-CESM55 simulation with the large refined patch of 0.5°, and quadrupled to ∼4300 core hours for the

VR-CESM28 simulation with the addition of the smaller 0.25° patch. By comparison, the computational cost of limited area model RACMO2 at 11 km is ∼6800 core hours per simulated year (Brice Noël, pers. comm.). The throughput was ∼25, ∼13 and ∼10 simulated years per day, for Uniform CESM, VR-CESM55, and VR-CESM28, respectively.

2.2 Reference data

Model results are quantitatively compared to accumulation and ablation observations (remotely-sensed and in-situ) and RCM output. CESM and RCM model data are taken from 1980-1999, a period prior to the onset of persistent circulation change and a strong decline in GrIS SMB in the 2000s (Fettweis et al., 2013b; van den Broeke et al., 2016). The field data analysis has been partly carried out in the Land Ice Verification & Validation Toolkit (LIVVkit), an open source software package designed for evaluating ice sheet models (Kennedy et al., 2017; Evans et al., 2018). For details on how model coordinates are mapped to the observations, the reader is referred to Evans et al. (2018).

Airborne accumulation radar data from NASA's Operation IceBridge are used to evaluate modelled accumulation rates in the GrIS interior, described in detail by Lewis et al. (2016). There are 18,968 values in this dataset, available as a seasonal average over one or more time periods. Following Evans et al. (2018), a simple time average is applied over all available periods for each record to yield a single accumulation value (in mm w.e. yr^{-1}) per location.

In-situ measurements of SMB (in mm w.e. yr^{-1}) are split into accumulation zone (SMB > 0) and ablation zone (SMB < 0) subsets. The accumulation zone collection is made up out of 421 firn core/snow pit/stake measurements taken from various field campaigns (Cogley, 2004; Bales et al., 2009; Evans et al., 2018). The ablation zone collection is a subset of the compilation of GrIS ablation zone SMB measurements by Machguth et al. (2016). Each record location is averaged in time to yield an annual SMB estimate. Only records that are on the CISM ice mask and have a record length equal or close (i.e., within 5%) to a full year are kept, which brings the total number of records down from 627 to 142, spread over 22 rather than 46 glaciers. It is important to mention at this point that the spatial coverage of the ablation zone measurements is quite sparse. This can be seen from Figure 1 in Evans et al. (2018), which shows that all ablation data stem from only 8 transects in total.

The regional climate model used is the Royal Netherlands Meteorological Institute (KNMI) regional atmospheric climate model (RACMO) version 2.3p2 (RACMO2 hereafter) at 11 km, a state-of-the-art polar climate model that has been extensively evaluated over the GrIS (Noël et al., 2018, 2015) and compares favourably to observations. At its lateral boundaries, RACMO2 was forced using ERA-Interim reanalysis data. The 11 km RACMO2 fields, notably runoff, have been statistically downscaled to a resolution of 1 km in order to better resolve narrow ablation zones and low-lying regions (Noël et al., 2016, 2018). For the purpose of this work, it is considered fair to compare VR-CESM directly to the downscaled RACMO2 product as (i) CESM also performs on-line downscaling using the semi-statistical elevation classes, and (ii) the best-estimate data would be used in order to identify possible model improvements or deficits, which is in line with the purpose of this paper.

The Cryosphere Discuss., https://doi.org/10.5194/tc-2018-257
Manuscript under review for journal The Cryosphere
Discussion started: 6 December 2018

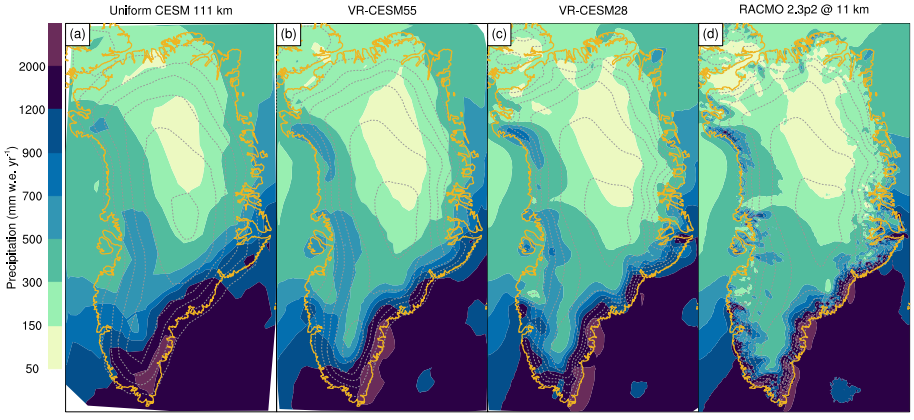

Figure 3. Spatial distribution of mean annual precipitation. Note the non-linear colour scale. CESM data are displayed at the native CAM resolution for the period 1980-1999. RACMO2 data are shown at native 11 km resolution for the same period. Coastlines and 500 m elevation contours are overlain in orange and grey, respectively.

3 Results

3.1 Precipitation

Steep edges of ice sheets as well as topographic promontories are effective drivers of orographic precipitation, as is apparent from the RACMO2 precipitation field (Figure 3d). The largest source of moisture is the North Atlantic basin, which is connected to Greenland by large-scale storm systems (Sodemann et al., 2008). Cyclonic activity associated with the persistent Icelandic Low drives warm and moist air onto land from the south-east, resulting in strong orographic uplift which causes rapid cooling, condensation, and precipitation. By comparison, northern Greenland is much drier with accumulation rates locally below 100 mm yr^{-1} (Cogley, 2004).

Since orographic precipitation is so dominant over southern Greenland, it is not surprising that we find significant improvements with increasing resolution, compared with RACMO2 (Figure 3). At uniform 111 km resolution, CESM correctly predicts a band of high (> 1000 mm yr^{-1}) precipitation rates in the south-east, however it extends too far into the interior (panel a). This is attributed to the fact that the poorly resolved topography is ∼600 m lower in the model than in reality (Figure 2) and that topographic gradients are smoothed out, which weakens the effect of orographic uplift. The VR-CESM55 result (panel b) shows that this is mostly a resolution issue as the band of high precipitation rates is more confined to the low-lying areas and slopes, similar to RACMO2. Other effects that can be seen in this VR-CESM55 result is the emergence of orographic precipitation in other locations around the margins, however weak, and a general drying of the northern interior. In VR-CESM28, similar resolution dependent patterns continue to emerge, with even stronger orographic precipitation and more pronounced drying in the north. Integrated over the entire GrIS, including peripheral glaciers and ice caps, precipitation is reduced from 946 ± 107 Gt yr^{-1} (Uniform CESM) to 823 ± 55 (VR-CESM55) and 806 ± 61 Gt yr^{-1} (VR-CESM28). Next, we look into accumulation and carry out a more quantitative analysis using the available reference data (Section 2.2).

The Cryosphere Discuss., https://doi.org/10.5194/tc-2018-257
Manuscript under review for journal The Cryosphere
Discussion started: 6 December 2018

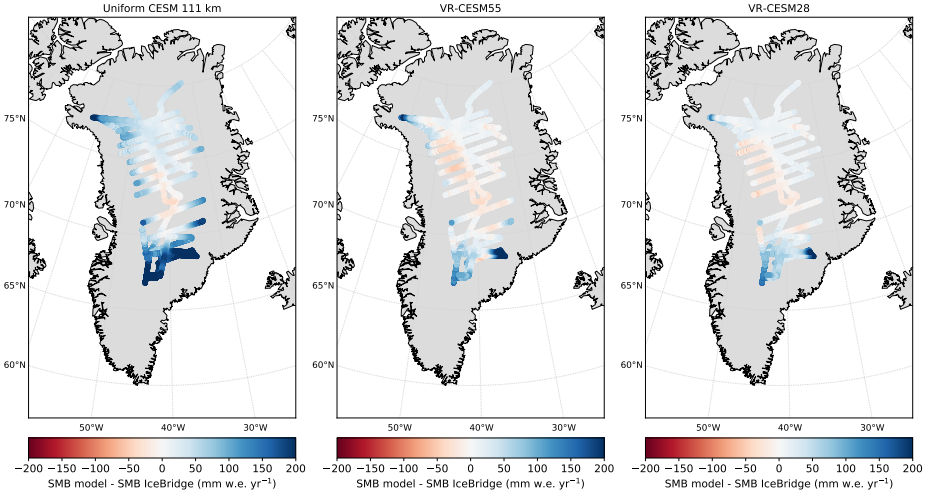

Figure 4. Accumulation difference CESM - IceBridge. Blue (red) colours indicate that the model is wetter (dryer) than observations.

3.2 Accumulation (IceBridge)

The IceBridge radar data supports the pattern of interior drying with increasing resolution. In Uniform CESM at 111 km resolution,we find a wet bias of 81 mm yr^{-1} which is most pronounced in regions near the edges of the IceBridge domain (Figure 4). The strongest wet bias is found in the south, where precipitation rates are highest (Figure 3) which means that any relative error will lead to a greater absolute error. Distributions of point-by-point deviations are depicted in Figure 5a. Here it can be seen that with increasing resolution, the mean bias drops from 81 mm to 22 mm (VR-CESM55) and 21 mm (VR-CESM28), which suggests that the largest improvement is made going from 111 to 55 km. At the same time the spread of deviations decreases with resolution, i.e. the distribution narrows. For instance, the 95th percentile, as a one-sided measure for this spread, falls from 298 mm to 122 mm (VR-CESM55) and 96 mm (VR-CESM28). IceBridge data suggest that a relatively small dry bias starts to develop in the western GrIS at higher resolutions (Figure 4). The corresponding 5th-percentiles of the point-by-point deviations are -12 mm (Uniform CESM), -28 mm (VR-CESM55) and -20 mm (VR-CESM28). As a result, the root mean squared error (RMSE) in VR-CESM55 (VR-CESM28) is reduced by 56% (65%) with respect to the uniform resolution, and the coefficient of determination r^2 is enhanced by 0.1 (0.15) (Table 1).

3.3 Accumulation (in-situ measurements)

Next, a similar analysis is carried out for the in-situ accumulation zone observations. Compared to the airborne radar data, these measurements cover a greater portion of the GrIS (cf. Figure 1 in Evans et al., 2018), including the southern dome, which makes it arguably more representative of the GrIS as a whole, although the spatial density is smaller. As before, the greatest absolute improvement is found in the doubling of resolution from 111 km to 55 km, with smaller benefits going further to 28 km (Figure 5b). The mean bias is halved (-107 mm) going from the uniform 111 km resolution to 55 km, and is further reduced by 30 mm

The Cryosphere Discuss., https://doi.org/10.5194/tc-2018-257
Manuscript under review for journal The Cryosphere
Discussion started: 6 December 2018

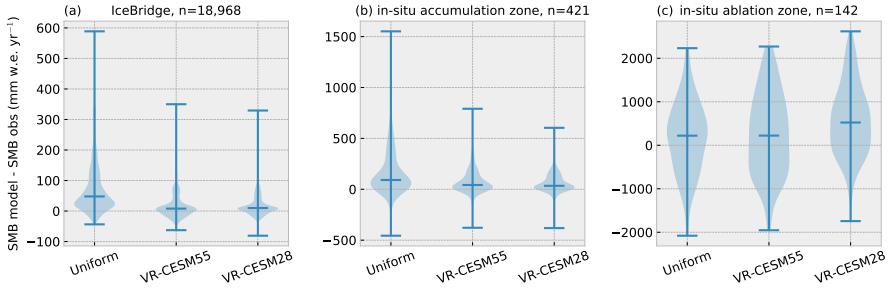

Figure 5. Distribution of point-by-point SMB differences between model (at 4 km) and observations. Horizontal lines indicate high/low maxima and median, respectively. Note the different scales.

Table 1. Statistics of CESM simulations (at 4 km) with respect to reference data (IceBridge, in-situ accumulation zone, in-situ ablation zone). Shown are mean bias, coefficient of determination, and root mean square error (RMSE). All values are significant in the two-sided Student's t-test (p<0.01). On each metric, the best ranking CESM simulation is highlighted in bold. The reference data are described in the text.

	IceBridge ($n = 18,968$)			In-situ Acc. ($n = 421$)			In-situ Abl. ($n = 142$)		
	bias (mm)	r^2	RMSE (mm)	bias	r^2	RMSE	bias	r^2	RMSE
Uniform CESM 1°	81.3	0.78	126	187	0.61	319	**184**	0.67	**846**
VR-CESM55 / 0.5 °	22.2	0.88	55.7	79.6	0.74	150	251	0.66	970
VR-CESM28 / 0.25 °	**21.4**	**0.93**	**44.7**	**63.4**	**0.79**	**120**	574	**0.70**	995

to 63 at 28 km (Table 1). This pattern of marginal returns is also reflected in RMSE (53% vs 62% decrease) and r^2 (+0.13 vs +0.18) for the VR-CESM55 and VR-CESM28 simulations, respectively. To put the numbers in Table 1 in perspective, Noël et al. (2018) reports a mean bias for RACMO2 of -22 mm and an RMSE of 72 mm for their accumulation zone measurements (version 2.3p2, their Figure 11a), and $r^2 = 0.85$. The bias in VR-CESM28 is still three times that of RACMO2, but the RMSE and r^2 are comparable.

3.4 Ablation (in-situ measurements)

High up on the ice sheet, and thus deep into the accumulation zone, SMB is dominated by snowfall. In the ablation zone, by contrast, there is a delicate balance between different factors — snowfall, sublimation, snowmelt, refreezing, and runoff — that complicates SMB modelling. Furthermore, SMB gradients are typically much stronger in the ablation zone than they are in the accumulation zone, mainly due to steep topography and non-linearity of SMB with height (Figure 6). Therefore, as one therefore expects, model skill in the ablation zone is lower than in the accumulation zone, with errors exceeding 2000 mm (Figure 5c) at some locations. Still, the coefficient of determination is reasonable ($r^2 > 0.65$ for all simulations, Table 1) and ablation zones are mostly predicted in the right locations (Figure 6), owing to the elevation class subgrid parameterization (Section 2.1.2).

The Cryosphere Discuss., https://doi.org/10.5194/tc-2018-257
Manuscript under review for journal The Cryosphere
Discussion started: 6 December 2018

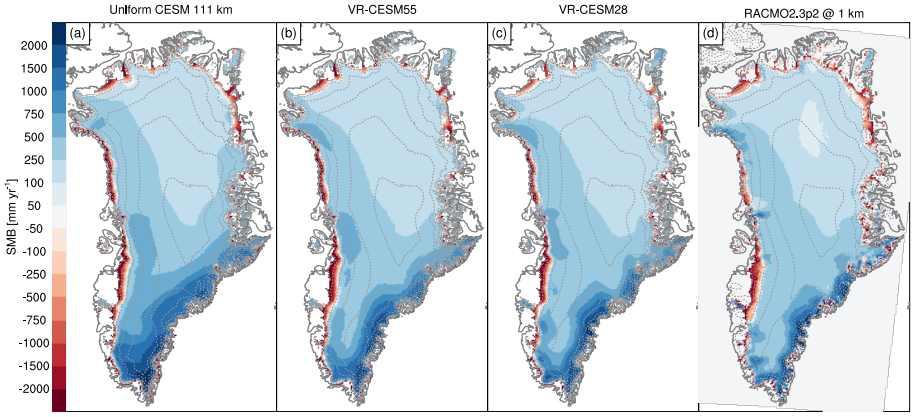

Figure 6. Mean annual SMB in mm yr^{-1}. All CESM data are downscaled to 4 km CISM resolution for the period 1980-1999. RACMO2 data have been statistically downscaled from 11 to 1 km. Note the non-linear colour scale.

Table 2. Mean GrIS mass fluxes for the period 1980-1999 in gigatonnes per year with standard deviation between brackets. The area of integration is listed in the first column and includes peripheral glaciers and ice caps. CESM data are integrated at the native resolution with elevation class weighing. The statistically downscaled 1 km RACMO2 data is averaged over the same period and described in Noël et al. (2018). RACMO2 does not differentiate between snow and ice melt in its output files so only total melt is reported.

Model name	Ice area	Precipitation	Ice melt	Total melt	Refreezing	Runoff	Sublimation	SMB
	km^2	Gt yr^{-1}	Gt yr^{-1}	Gt yr^{-1}	Gt yr^{-1}	Gt yr^{-1}	Gt yr^{-1}	Gt yr^{-1}
Uniform CESM 1°	1,812,467	946 (107)	217 (48)	468 (100)	178 (43)	349 (67)	28 (3)	567 (129)
VR-CESM55 / 0.5 °	1,812,254	823 (55)	179 (46)	447 (108)	191 (49)	300 (69)	39 (4)	485 (93)
VR-CESM28 / 0.25 °	1,812,254	806 (61)	142 (52)	384 (104)	183 (42)	248 (74)	44 (5)	514 (97)
RACMO2 1 km	1,761,475	743 (64)	-	577 (81)	309 (27)	344 (68)	33 (2)	365 (109)

Different to accumulation zone, model skill in the ablation zone does not improve with resolution (Table 1). The mean bias deepens from 184 mm (Uniform CESM) to 251 mm (VR-CESM55) and 574 mm (VR-CESM28), which are increases of 36 % and 212 %, respectively. The r^2 is similar across all simulations, with the largest value of 0.70 for simulation VR-CESM28. The RMSE is slightly increased in both VR simulations to 970 mm (+15 %) and 995 mm (+18 %), respectively. To put these numbers in perspective again, Noël et al. (2018) reports a mean bias for RACMO2 of 120 mm and an RMSE of 870 mm for their ablation zone measurements (version 2.3p2 downscaled to 1km, their Figure 11c), and $r^2 = 0.72$. We note that although the bias is larger in all our CESM simulations, RMSE and r^2 are comparable. The bias in the ablation zone of the non-downscaled RACMO2 is 600 mm (Noël et al. (2018), their Figure 11b).

The Cryosphere Discuss., https://doi.org/10.5194/tc-2018-257
Manuscript under review for journal The Cryosphere
Discussion started: 6 December 2018

3.5 Integrated SMB (regional climate model data)

The main SMB components are integrated over their respective ice masks and listed in Table 2. Compared to the 1-km statistically downscaled RACMO2 data, all CESM simulations overestimate GrIS-integrated precipitation. The bias in precipitation is largest for Uniform CESM (203 $\pm$ 125 Gt yr^{-1}, or +27 %) and reduces to 11 % (VR-CESM55) and 8 % (VR-CESM28) which is in line with our earlier findings of progressive drying with increased resolution. Part of remaining bias may be related to the $\sim$ 3 % larger ice sheet extent in CESM, relative to RACMO2.

Melt, on the other hand, is consequently underestimated in all CESM simulations (Table 2). The bias of total melt volume is smallest for coarse-resolution Uniform CESM (-19 %) and largest for fine-resolution run VR-CESM28 (-34 %), which is consistent with the findings presented in the previous section on ablation zone measurements. Going from Uniform CESM at 111 km to VR-CESM55 the reduction in ice melt (38 Gt $\pm$ 66) exceeds the reduction in total melt (21 $\pm$ 147), which must mean that snow melt is increasing. This is no longer the case at the next resolution doubling (VR-CESM28) where both ice and snow melt are reduced. The enhanced snow melt in VR-CESM55 helps to explain why total refreezing is largest in this simulation (Table 2), although the differences across the CESM simulations are small.

In CESM, surface runoff is the sum of bare ice melt and drainage from the bottom of the snow pack, i.e. liquid water originating from rain or melt that does not refreeze. Due to the reductions in total melt volume, runoff is also significantly reduced at higher resolutions (Table 2), leading to large biases when compared against the downscaled 1 km RACMO2 data. A small positive bias in Uniform CESM (5 Gt $\pm$ 95 Gt) drops to negative biases in VR-CESM55 (-44 $\pm$ 97 Gt) and VR-CESM28 (-96 $\pm$ 100 Gt).

To investigate further the spatial variability of runoff, we computed total runoff across 7 GrIS basins, derived from an updated ice flow mosaic of Rignot and Mouginot (2012). The results can been seen in Figure 7. CESM runoff is monotonically decreasing with increasing resolution in all regions except region 5 and 6. In the northern and eastern parts of the GrIS (basins 1, 2 and 3) this leads to a deeper negative bias with respect to RACMO2. In these basins, the mean runoff as simulated by VR-CESM28 is in fact outside the range of one RACMO2 standard deviation, in contrast to Uniform CESM which is still within that range in basin 1 and 3. In the south-east (basin 4), runoff is significantly overestimated in Uniform CESM. This is attributed to the poorly resolved precipitation field, which in reality exhibits steep gradients over this region (see e.g. Figure 3). With increased precipitation at lower elevations, more meltwater can be buffered and less bare ice reaches the surface, thereby limiting runoff. The runoff simulated by VR-CESM55 falls within one standard deviation of the RACMO2 result. The largest absolute runoff flux is simulated in south-western basin 5. The results of this region are interesting because the response of runoff to resolution increase is not consistently in the same direction, which suggests that different, counter-acting mechanisms are active. Nevertheless, all CESM results fall within one standard deviation of RACMO2 due to the high variability in this region. Runoff in basins 6 and 7 is consistently overestimated in all CESM simulations with respect to RACMO2, but less so at higher resolutions.

At this point it is worth reiterating that the comparison to RACMO 2.3p2 downscaled data at 1 km Noël et al. (2018) is a rather stringent test. Nevertheless, these benchmark data are also subject to uncertainty. Noël et al. (2018) characterise the

The Cryosphere Discuss., https://doi.org/10.5194/tc-2018-257
Manuscript under review for journal The Cryosphere
Discussion started: 6 December 2018

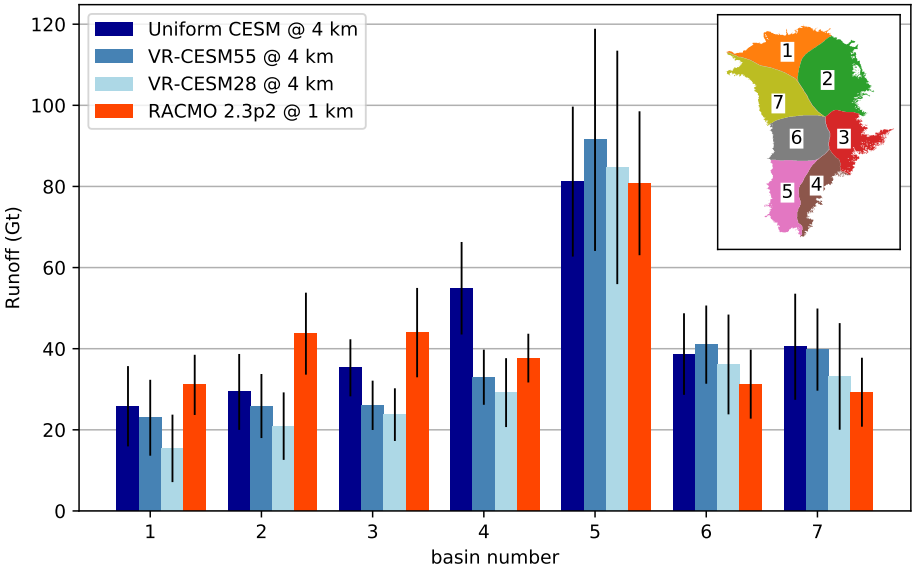

Figure 7. Basin-wide runoff for the period 1980-1999. Error bars represent one standard deviation. CESM data have been bi-linearly interpolated down from their native resolution to 4 km while making using the vertical elevation class output. The (already downscaled) RACMO2 data have been processed at their native 1 km resolution. The total runoff across all basins differs from the value reported in Table 2 due to differences in ice extent, since the basins only cover the contiguous ice sheet (total area 1,700,772 km^2).

native spatial resolution of 11 km as a source of model uncertainty, as well as the representation of surface roughness and surface albedo. Two prime uncertainties in the RACMO2 downscaling procedure arise from the bare ice albedo used to correct runoff, and the ice sheet extent (Noël et al., 2016).

Finally, sublimation is enhanced in both VR runs compared to Uniform CESM (Table 2) which is attributed to the higher wind speeds that are present in the VR-CESM simulations (not shown). In VR-CESM28, the increase relative to Uniform CESM is largest and exceeds 50 %. Still, sublimation is a relatively minor term in the surface mass budget of the GrIS.

To conclude, the GrIS integrated SMB is consistently overestimated in all CESM simulations relative to the downscaled RACMO2 data. As discussed above, there are different leading terms underpinning this bias in each simulation. In Uniform CESM and VR-CESM55, the SMB component with the largest deviation from the reference data is precipitation, with comparably minor biases in runoff and sublimation. Precipitation is better resolved in VR-CESM28 which therefore compares more favourably to RACMO2 in a GrIS-integrated sense. In this simulation, however, runoff is more strongly biased than in the other simulations, such that it is now the SMB component with the largest absolute deviation. The basin analysis indicated that runoff is particularly biased in the north and north-eastern regions of the GrIS. Out of the three CESM simulations, VR-CESM55 has an integrated SMB value most similar to RACMO2, with a positive bias of 120 $\pm$ 143 Gt (Table 2).

The Cryosphere Discuss., https://doi.org/10.5194/tc-2018-257
Manuscript under review for journal The Cryosphere
Discussion started: 6 December 2018

4 Discussion

One important and perhaps unexpected finding of the previous section is that melt and runoff generally decrease at higher resolutions, deteriorating the agreement with the – albeit sparse – ablation zone measurements. Here, we aim to identify possible driving mechanisms in an attempt to understand what might be causing this behaviour.

The first candidate for such a mechanism, naturally, is the redistribution of precipitation. At the margins, local increases in snowfall occur due to the steeper terrain at higher resolution (Figure 2), enhancing orographic uplift and condensation. More winter snow means delayed bare-ice exposure in summer and an increased refreezing capacity in spring and autumn. Moreover, summer snowfall is potentially even more important since it can cover dark bare ice with bright fresh snow and interrupt the snow-albedo-melt feedback (Noël et al., 2015). But precipitation does not explain everything.

In particular, the comparison with the RACMO2 data indicated that runoff in VR-CESM28 is most markedly underestimated in the northern and north-eastern basins of the GrIS (Figure 7), where precipitation does not change substantially at higher resolution. . In this region, low precipitation rates in combination with high wind speeds lead to a high contribution of blowing snow processes to SMB. Therefore, even state-of-the-art regional climate models, such as RACMO2, struggle to capture the SMB of the northern GrIS. For example, blowing snow was overestimated in a previous version of RACMO2 (RACMO 2.3p1), causing a too-wide ablation zone in the north (Noël et al., 2018). Here, CESM simulates an ablation zone that is too narrow in all three simulations (Figure 6), which may be explained by the fact that neither drifting snow redistribution, nor sublimation are included in CESM (van Kampenhout et al., 2017).

4.1 Large-scale circulation

Another important driving mechanism for runoff changes could be a shift/change in the large-scale atmospheric circulation induced by the resolution changes, leading to lower tropospheric temperatures over Greenland and an associated reduced downwelling longwave flux at the surface. To this end, we compared CESM mid-troposphere geopotential height and temperature across the different resolutions. Circulation anomalies are computed by subtracting the Uniform CESM fields from VR-CESM55 and VR-CESM28, respectively, which is done after regridding to a common mesh. The resulting anomaly maps in 500 hPa summer (JJA) geopotential height (Z500) and temperature (T500) are depicted in Figure 8.

In both VR-CESM simulations, positive Z500 anomalies (increased heights) are apparent over the north-east Atlantic Ocean and the Bering Strait, with negative anomalies elsewhere in the Arctic. The broad similarity between the anomaly patterns in both VR-CESM runs makes it unlikely that internal variability is responsible for generating these patterns, so we interpret these patterns as actual large-scale circulation changes. This claim is further supported by anomaly fields in the other seasons, which also indicate consistent circulation patterns across both VR-CESM simulations (not shown). Therefore we conclude that these changes are due to the subsequent refinement of topography over Greenland (Figure 2) and elsewhere within the VR domain (Figure 1). The higher (and steeper) topography promotes atmospheric blocking and leads to disturbances in the near-stationary Rossby / planetary waves and is an example of the upstream / downstream impacts that the VR-CESM approach captures, which may not otherwise be present in offline RCM dynamical downscaling.

The Cryosphere Discuss., https://doi.org/10.5194/tc-2018-257
Manuscript under review for journal The Cryosphere
Discussion started: 6 December 2018

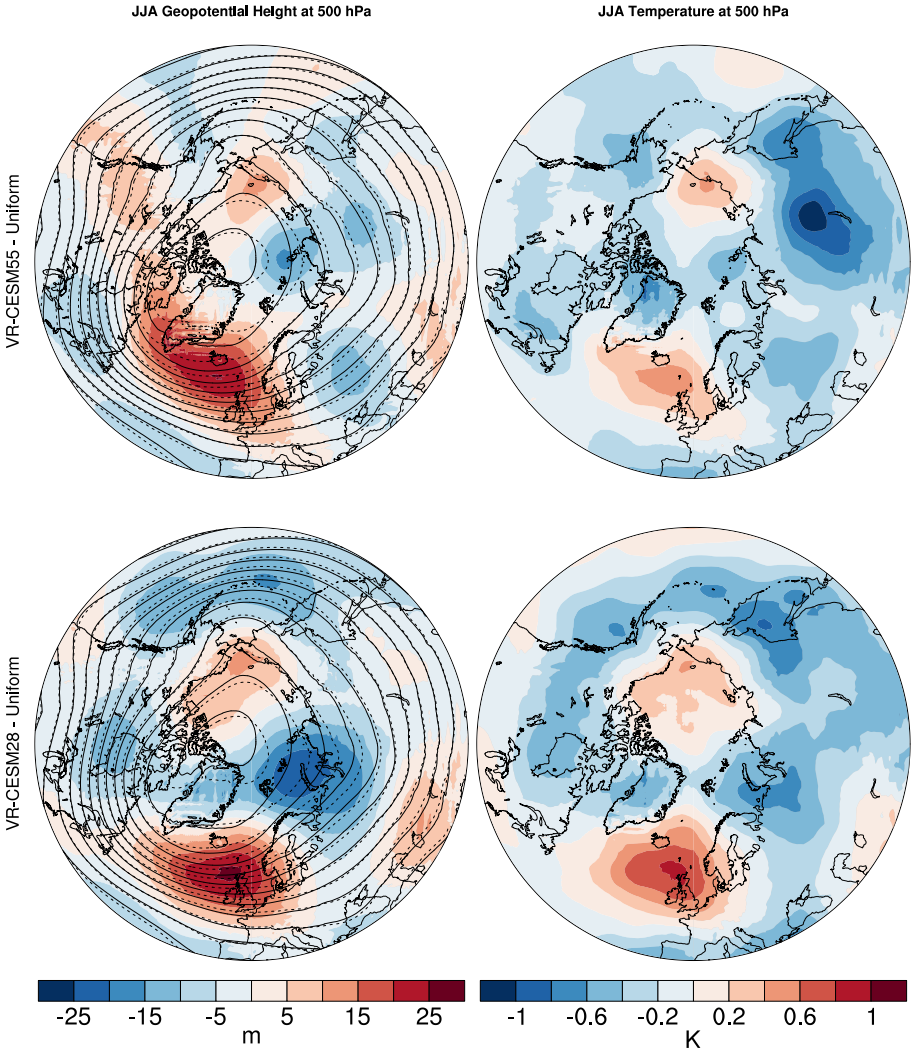

Figure 8. Changes in large-scale circulation and mid-troposphere temperature between VR-CESM and uniform resolution CESM. Solid lines represent Z500 from the Uniform CESM run, dashed lines represent VR-CESM Z500, both drawn at 20 m intervals. Prior to subtraction, all data have been regridded to a common regular mesh of 0.25° using bi-linear interpolation.

Over Greenland, decreased geopotential height indicates more cyclonic flow, drawing in cold air from the Arctic ocean. By and large, anomalies in summer T500 are fairly well correlated with anomalies in Z500, which suggests that the changes in T500 are predominantly forced by circulation (Figure 8). Summer T500 anomalies ranging from -0.2 to -0.6 K are found across Greenland. This indicates that, indeed, large scale circulation changes are likely an important driver of the lower melt and runoff rates found at higher resolutions.

The Cryosphere Discuss., https://doi.org/10.5194/tc-2018-257
Manuscript under review for journal The Cryosphere
Discussion started: 6 December 2018

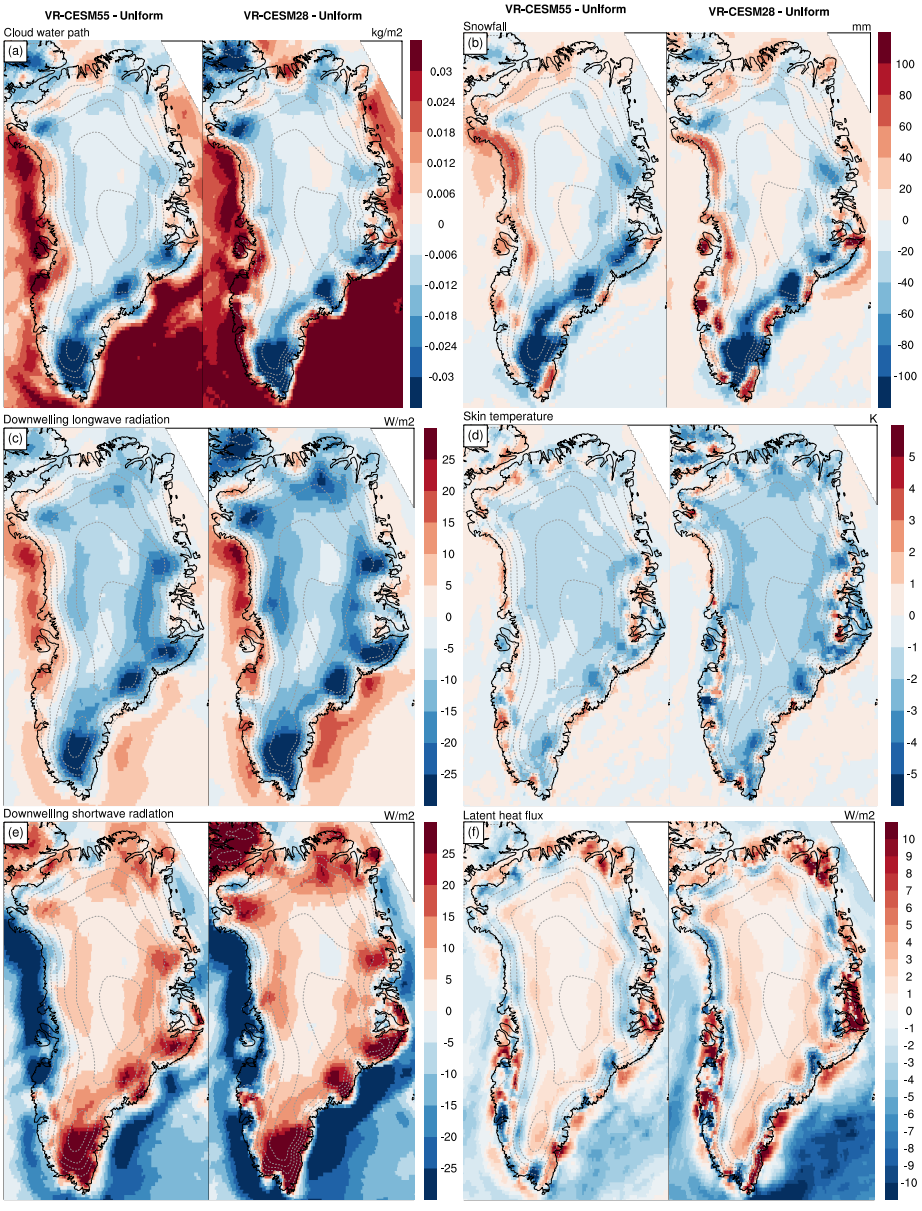

Figure 9. Summer (JJA) anomalies of selected variables. Prior to subtraction, all data have been regridded to a common regular mesh of 0.25° using bi-linear interpolation. The anomaly map for 2-m air temperature (not shown) is similar to that of the skin temperature (panel d).

4.2 Clouds and radiation

Next, the role of cloud cover is investigated. Clouds are an important modulator of the surface energy balance and therefore melt and runoff. Anomalies of summer cloud water path of both VR-CESM simulations have been computed and are displayed in Figure 9a. Cloud water path exhibits negative anomalies – implying that VR-CESM clouds contain less water and ice than

their counterparts in the Uniform CESM simulation – in places of reduced precipitation (Figure 9b). Positive anomalies are mainly found over the open ocean and close to the margins, where locally the terrain has lowered due to the better resolved height gradients (Figure 2). More importantly, negative anomalies are also found across most of the northern and eastern parts of the GrIS. Likely, this is a combination of topographic effects and circulation changes, through which less moisture is brought to the region.

As a result of both the reduced cloud content and the colder ambient troposphere (Figure 8), downwelling longwave radiation is significantly reduced. In VR-CESM28, anomalies below -10 W m^2 are found across large areas in the north and east (Figure 9c). We argue that this must be the leading cause for the $\sim$1 K skin temperature anomaly found across most of the GrIS (Figure 9d). This temperature decrease is most likely to impact melt in areas that are already cold (the north) and see a relatively short melt season. This is in line with other studies that showed that longwave radiation from clouds is a dominant factor for initiation of melt and extreme melt events in cold regions of the ice sheet (e.g. (Bennartz et al., 2013; Van Tricht et al., 2016; Cullather and Nowicki, 2018)).

Reduced cloud cover in general also increases downwelling shortwave radiation received by the surface, here shown in Figure 9e. The magnitude of the insolation anomaly is comparable to that of the longwave flux, but it is still modulated by the high surface albedo. Therefore, we conclude that the net effect of all incoming radiation on the surface energy balance is negative, except for locations where albedo is low.

4.3 Latent heat

Higher summer wind speeds in both VR-CESM simulations (not shown) enhance sublimation along the GrIS margins, which acts as a surface energy sink in the ablation zone (Figure 9f). In response, less energy is available for warming the surface through sensible heat and surface melting.

4.4 Subgrid downscaling

The multiple elevation classes method introduced by Lipscomb et al. (2013) as a means of subgrid downscaling (see Section 2.1.2) gradually becomes less important when resolution is increased, since the topographic variability within a single grid cell is smaller. We hypothesise that a bias in the lapse rates used in the meteorological downscaling has the potential to bias the CESM runoff results, especially at coarser resolutions.

4.5 Summary

Several potential driving mechanisms have been proposed that each may explain the reduced melt and runoff fluxes found at higher CESM resolutions. Since some of these processes are intertwined, e.g. the role of cloud cover and tropospheric temperature on downwelling longwave radiation, based on the available data it is not possible to quantify their individual contributions. Only a full reconstruction of the surface energy balance in monitored sites could shed further light on that.

However, this is deemed outside of the scope of the current study, which is intended as an exploratory first step in applying VR-CESM to Greenland.

5 Limitations

Unfortunately, a mistake was found in the land cover input file that was used in both VR-CESM simulations, but not in the Uniform CESM run. The faulty input files led to the unphysical release of sensible heat into the lower atmosphere during bare ice melt conditions. The additional amount of sensible heat released equals the melt energy that was generated in the same time step. It is noted that the magnitude of the erroneous energy flux is equivalent to a similar flux common over non-glaciated surfaces (i.e. that cannot melt), except that here it is released as sensible heat rather than e.g. outgoing longwave radiation. Since our results suggest a lack of bare ice melt in VR-CESM, rather than an excess, this error does not impact the main conclusions of this study.

Little attention has been given in this study to the degree in which internal variability affects Greenland SMB. Compared to RCMs, which are both forced at the domain edge and ocean surface, there is relatively weak "weather" forcing in our atmosphere-only CESM simulations. Arguably, a model run of 20 years is not quite long enough to attain a robust mean climate. Therefore, the numbers presented in Table 2 should be used with some caution. We plan on doing a follow-up study where the impact of atmospheric variability on Greenland SMB in AMIP simulations is diagnosed.

The difference in ice masks between RACMO2 and CESM remains another source of uncertainty, especially when calculating GrIS integrated numbers like in Table 2. In follow-up studies it is therefore recommended to use overlapping masks, or to distinguish between the contiguous GrIS and peripheral glaciers and ice caps. Unfortunately, neither CLM nor CISM currently provide such a distinction, so a workaround solution may be needed. In the case of runoff, the peripheral contribution in CESM could be estimated by computing the integrated runoff over the different basins (Figure 7). The drawback is that these numbers are calculated using bi-linear interpolation and are not necessarily very accurate.

6 Summary and Conclusions

For the first time, regionally refined GCM simulations using VR-CESM have been performed at 55 & 28 km over the greater Greenland region to study the impact of resolution on GrIS SMB. Compared to a uniform resolution (1° or ∼111 km) control run, topography is resolved with greater fidelity leading to improved patterns in orographic precipitation, most notably in southern Greenland and along the western and eastern margins. At the same time, a general drying in the GrIS interior occurs, which significantly improves correlations to IceBridge accumulation radar and in-situ measurements of accumulation. Arguably, VR-CESM28 now performs on-par with RCMs in these regions (Lewis et al., 2016). In transient simulations, the improved distribution of snowfall may prove pivotal as it modulates the timing and strength of the snow-albedo feedback (Picard et al., 2012) and ice advection. GrIS integrated precipitation is reduced to 806 Gt in VR-CESM28, which is more in line with best-estimate RCM figures.

In the ablation zone, the CESM simulations were evaluated using geographically sparse in-situ measurements. Despite its coarse resolution of ∼111 km, we found that Uniform CESM reproduces these measurements to a reasonable degree, which due to the complexity of ablation zone could be a fortuitous combination of compensating biases, but may also indicate the effectiveness of multiple elevation classes in CESM (Lipscomb et al., 2013). By comparison, both VR-CESM simulations show an increasingly large positive SMB bias, indicating too little ablation. This is reflected in their GrIS-wide integrated melt and runoff fluxes, which are substantially lower in VR-CESM28 than in Uniform CESM. A basins-by-basin analysis revealed that the largest reductions in runoff are found in the northern and eastern basins.

Several driving mechanisms were explored that could be underpinning these reductions. It was shown that the topographic changes on Greenland and in the rest of the domain causes large-scale circulation changes which, as a result, led to lower 500 hPa summer temperatures over the GrIS. Combined with local reductions in cloud cover, this affects the radiative budget at the surface, in particular the downwelling longwave flux, leading up to a decrease in skin temperature by 1–2 K. Enhanced sublimation by higher wind speeds at increased resolution are hypothesised to play a role as well, drawing away energy from the surface energy budget.

Several possible avenues for future research are suggested; (1) with a focus on large-scale circulation, one could compare tropospheric conditions in VR-CESM to reanalyses and alleviate potential biases by tuning relevant atmospheric parameters; (2) one could explore yet higher VR resolutions, like 14 or 7 km Rhoades et al. (2018), and study the impact on Greenland SMB; (3) drifting snow sublimation and redistribution could be implemented and evaluated over the GrIS using VR-CESM; (4) as of present it is not possible to run VR-CESM with an active ocean model. Still, projections on future GrIS SMB could be generated using VR-CESM when high-frequency output from fully-coupled scenario simulations are used as boundary conditions to VR-CESM.

To conclude, our study shows that VR-CESM is a viable technique for dynamically downscaling GCM climate simulations, while maintaining model consistency and allowing for feedbacks between the region of interest and the rest of the globe. A finer resolution leads to better resolved storms that are taking different pathways than their low-resolution counterparts, and therefore change precipitation and cloud cover patterns on a local scale. VR-CESM can serve as a tool for modellers that are interested in the dynamical response of the GrIS to future SMB changes since VR-CESM can be coupled to ice sheet models like CISM.

Data availability. All climate model data used in the analyses are available on Zenodo under DOI (to be done before publication)

Author contributions. LK and MRB originally conceived the study. The simulations were set up and carried out by LK and AMR with help from ARH and CMZ. LK led the writing of the manuscript, with contributions from all the other authors.

Competing interests. The authors declare no competing interests.

Acknowledgements. The authors thank Paul Ullrich (UC Davis) and Aarnout van Delden (UU/IMAU) for useful discussions and Brice Noël (UU/IMAU) for sharing the RACMO2 data used. This work was carried out under the program of the Netherlands Earth System Science Centre (NESSC), financially supported by the Ministry of Education, Culture and Science (OCW, Grantnr. 024.002.001). Author Rhoades was funded by the U.S. Department of Energy, Office of Science "An Integrated Evaluation of the Simulated Hydroclimate System of the Continental US" project (award no. DE-SC0016605).

References

Bales, R. C., Guo, Q., Shen, D., McConnell, J. R., Du, G., Burkhart, J. F., Spikes, V. B., Hanna, E., and Cappelen, J.: Annual Accumulation for Greenland Updated Using Ice Core Data Developed during 2000–2006 and Analysis of Daily Coastal Meteorological Data, Journal of Geophysical Research: Atmospheres, 114, https://doi.org/10.1029/2008JD011208, 2009.

Beljaars, A. C. M., Brown, A. R., and Wood, N.: A New Parametrization of Turbulent Orographic Form Drag, Q.J.R. Meteorol. Soc., 130, 1327–1347, https://doi.org/10.1256/qj.03.73, 2004.

Bennartz, R., Shupe, M. D., Turner, D. D., Walden, V. P., Steffen, K., Cox, C. J., Kulie, M. S., Miller, N. B., and Pettersen, C.: July 2012 Greenland Melt Extent Enhanced by Low-Level Liquid Clouds, Nature, 496, 83–86, https://doi.org/10.1038/nature12002, 2013.

Cogley, J. G.: Greenland Accumulation: An Error Model, Journal of Geophysical Research: Atmospheres, 109, https://doi.org/10.1029/2003JD004449, 2004.

Cullather, R. I. and Nowicki, S. M. J.: Greenland Ice Sheet Surface Melt and Its Relation to Daily Atmospheric Conditions, Journal of Climate, 31, 1897–1919, https://doi.org/10.1175/JCLI-D-17-0447.1, 2018.

Cullather, R. I., Nowicki, S. M. J., Zhao, B., and Suarez, M. J.: Evaluation of the Surface Representation of the Greenland Ice Sheet in a General Circulation Model, Journal of Climate, 27, 4835–4856, https://doi.org/10.1175/JCLI-D-13-00635.1, 2014.

Delworth, T. L., Rosati, A., Anderson, W., Adcroft, A. J., Balaji, V., Benson, R., Dixon, K., Griffies, S. M., Lee, H.-C., Pacanowski, R. C., Vecchi, G. A., Wittenberg, A. T., Zeng, F., and Zhang, R.: Simulated Climate and Climate Change in the GFDL CM2.5 High-Resolution Coupled Climate Model, J. Climate, 25, 2755–2781, https://doi.org/10.1175/JCLI-D-11-00316.1, 2011.

Dennis, J. M., Edwards, J., Evans, K. J., Guba, O., Lauritzen, P. H., Mirin, A. A., St-Cyr, A., Taylor, M. A., and Worley, P. H.: CAM-SE: A Scalable Spectral Element Dynamical Core for the Community Atmosphere Model, The International Journal of High Performance Computing Applications, 26, 74–89, https://doi.org/10.1177/1094342011428142, 2012.

Evans, K. J., Kennedy, J. H., Lu, D., Forrester, M. M., Price, S., Fyke, J., Bennett, A. R., Hoffman, M. J., Tezaur, I., Zender, C. S., and Vizcaíno, M.: LIVVkit 2.1: Automated and Extensible Ice Sheet Model Validation, Geoscientific Model Development Discussions, pp. 1–31, https://doi.org/10.5194/gmd-2018-70, 2018.

Eyring, V., Bony, S., Meehl, G. A., Senior, C. A., Stevens, B., Stouffer, R. J., and Taylor, K. E.: Overview of the Coupled Model Intercomparison Project Phase 6 (CMIP6) Experimental Design and Organization, Geoscientific Model Development, 9, 1937–1958, https://doi.org/10.5194/gmd-9-1937-2016, 2016.

Fettweis, X., Franco, B., Tedesco, M., van Angelen, J. H., Lenaerts, J. T. M., van den Broeke, M. R., and Gallée, H.: Estimating the Greenland Ice Sheet Surface Mass Balance Contribution to Future Sea Level Rise Using the Regional Atmospheric Climate Model MAR, The Cryosphere, 7, 469–489, https://doi.org/10.5194/tc-7-469-2013, 2013a.

Fettweis, X., Hanna, E., Lang, C., Belleflamme, A., Erpicum, M., and Gallée, H.: Brief Communication "Important Role of the Mid-Tropospheric Atmospheric Circulation in the Recent Surface Melt Increase over the Greenland Ice Sheet", The Cryosphere, 7, 241–248, https://doi.org/10.5194/tc-7-241-2013, 2013b.

Fischer, R., Nowicki, S., Kelley, M., and Schmidt, G.: A System of Conservative Regridding for Ice-Atmosphere Coupling in a General Circulation Model (GCM), Geoscientific Model Development, 7, p. 883–907, https://doi.org/10.5194/gmd-7-883-2014, 2014.

Flanner, M. G. and Zender, C. S.: Snowpack Radiative Heating: Influence on Tibetan Plateau Climate, Geophysical Research Letters, 32, https://doi.org/10.1029/2004GL022076, 2005.

Gates, W. L., Boyle, J. S., Covey, C., Dease, C. G., Doutriaux, C. M., Drach, R. S., Fiorino, M., Gleckler, P. J., Hnilo, J. J., Marlais, S. M., Phillips, T. J., Potter, G. L., Santer, B. D., Sperber, K. R., Taylor, K. E., and Williams, D. N.: An Overview of the Results of the Atmospheric Model Intercomparison Project (AMIP I), Bull. Amer. Meteor. Soc., 80, 29–56, https://doi.org/10.1175/1520-0477(1999)080<0029:AOOTRO>2.0.CO;2, 1999.

Gettelman, A. and Morrison, H.: Advanced Two-Moment Bulk Microphysics for Global Models. Part I: Off-Line Tests and Comparison with Other Schemes, J. Climate, 28, 1268–1287, https://doi.org/10.1175/JCLI-D-14-00102.1, 2014.

Gettelman, A., Callaghan, P., Larson, V. E., Zarzycki, C. M., Bacmeister, J., Lauritzen, P. H., Bogenschutz, P. A., and Neale, R.: Regional Climate Simulations With the Community Earth System Model, Journal of Advances in Modeling Earth Systems, https://doi.org/10.1002/2017MS001227, 2018.

Guba, O., Taylor, M. A., Ullrich, P. A., Overfelt, J. R., and Levy, M. N.: The Spectral Element Method (SEM) on Variable-Resolution Grids: Evaluating Grid Sensitivity and Resolution-Aware Numerical Viscosity, Geosci. Model Dev., 7, 2803–2816, https://doi.org/10.5194/gmd-7-2803-2014, 2014.

Helsen, M. M., van de Wal, R. S. W., Reerink, T. J., Bintanja, R., Madsen, M. S., Yang, S., Li, Q., and Zhang, Q.: On the Importance of the Albedo Parameterization for the Mass Balance of the Greenland Ice Sheet in EC-Earth, The Cryosphere, 11, 1949–1965, https://doi.org/10.5194/tc-11-1949-2017, 2017.

Herrington, A. and Reed, K.: An Idealized Test of the Response of the Community Atmosphere Model to Near-Grid-Scale Forcing Across Hydrostatic Resolutions, Journal of Advances in Modeling Earth Systems, 10, 560–575, https://doi.org/10.1002/2017MS001078, 2018.

Howat, I. M., Negrete, A., and Smith, B. E.: The Greenland Ice Mapping Project (GIMP) Land Classification and Surface Elevation Data Sets, The Cryosphere, 8, 1509–1518, https://doi.org/10.5194/tc-8-1509-2014, 2014.

Huang, X., Rhoades, A. M., Ullrich, P. A., and Zarzycki, C. M.: An Evaluation of the Variable-Resolution CESM for Modeling California's Climate, J. Adv. Model. Earth Syst., 8, 345–369, https://doi.org/10.1002/2015MS000559, 2016.

Hurrell, J. W., Hack, J. J., Shea, D., Caron, J. M., and Rosinski, J.: A New Sea Surface Temperature and Sea Ice Boundary Dataset for the Community Atmosphere Model, J. Climate, 21, 5145–5153, https://doi.org/10.1175/2008JCLI2292.1, 2008.

Kennedy, J. H., Bennett, A. R., Evans, K. J., Price, S., Hoffman, M., Lipscomb, W. H., Fyke, J., Vargo, L., Boghozian, A., Norman, M., and Worley, P. H.: LIVVkit: An Extensible, Python-Based, Land Ice Verification and Validation Toolkit for Ice Sheet Models, Journal of Advances in Modeling Earth Systems, 9, 854–869, https://doi.org/10.1002/2017MS000916, 2017.

Lauritzen, P. H., Nair, R. D., Herrington, A. R., Callaghan, P., Goldhaber, S., Dennis, J. M., Bacmeister, J. T., Eaton, B. E., Zarzycki, C. M., Taylor, M. A., Ullrich, P. A., Dubos, T., Gettelman, A., Neale, R. B., Dobbins, B., Reed, K. A., Hannay, C., Medeiros, B., Benedict, J. J., and Tribbia, J. J.: NCAR Release of CAM-SE in CESM2.0: A Reformulation of the Spectral-Element Dynamical Core in Dry-Mass Vertical Coordinates with Comprehensive Treatment of Condensates and Energy, Journal of Advances in Modeling Earth Systems, 0, https://doi.org/10.1029/2017MS001257, 2018.

Lefebre, F., Fettweis, X., Gallée, H., Ypersele, J.-P. V., Marbaix, P., Greuell, W., and Calanca, P.: Evaluation of a High-Resolution Regional Climate Simulation over Greenland, Climate Dynamics, 25, 99–116, https://doi.org/10.1007/s00382-005-0005-8, 2005.

Leguy, G., Lipscomb, W. H., and Sacks, W. J.: CESM Land Ice Documentation and User Guide, https://escomp.github.io/cism-docs/cism-in-cesm/doc_work/html/, 2018.

Lenaerts, J. T., Vizcaino, M., Fyke, J., van Kampenhout, L., and van den Broeke, M. R.: Present-Day and Future Antarctic Ice Sheet Climate and Surface Mass Balance in the Community Earth System Model, Climate Dynamics, 47, 1367–1381, 2016.

Lewis, G., Osterberg, E., Hawley, R., Whitmore, B., and Marshall, H. P.: Regional Greenland Accumulation Variability from Operation IceBridge Airborne Accumulation Radar, The Cryosphere Discussions, pp. 1–29, https://doi.org/10.5194/tc-2016-248, 2016.

Ligtenberg, S. R. M., Kuipers Munneke, P., Noël, B. P. Y., and van den Broeke, M. R.: Brief Communication: Improved Simulation of the Present-Day Greenland Firn Layer (1960–2016), The Cryosphere, 12, 1643–1649, https://doi.org/10.5194/tc-12-1643-2018, 2018.

Lipscomb, W. H., Fyke, J. G., Vizcaíno, M., Sacks, W. J., Wolfe, J., Vertenstein, M., Craig, A., Kluzek, E., and Lawrence, D. M.: Implementation and Initial Evaluation of the Glimmer Community Ice Sheet Model in the Community Earth System Model, Journal of Climate, 26, 7352–7371, https://doi.org/10.1175/JCLI-D-12-00557.1, 2013.

Machguth, H., Thomsen, H. H., Weidick, A., Ahlstrøm, A. P., Abermann, J., Andersen, M. L., Andersen, S. B., Bjørk, A. A., Box, J. E., Braithwaite, R. J., Bøggild, C. E., Citterio, M., Clement, P., Colgan, W., Fausto, R. S., Gleie, K., Gubler, S., Hasholt, B., Hynek, B., Knudsen, N. T., Larsen, S. H., Mernild, S. H., Oerlemans, J., Oerter, H., Olesen, O. B., Smeets, C. J. P. P., Steffen, K., Stober, M., Sugiyama, S., As, D. V., Broeke, M. R. V. D., and Wal, R. S. W. V. D.: Greenland Surface Mass-Balance Observations from the Ice-Sheet Ablation Area and Local Glaciers, Journal of Glaciology, 62, 861–887, https://doi.org/10.1017/jog.2016.75, 2016.

Mottram, R., Boberg, F., Langen, P., Yang, S., Rodehacke, C., Christensen, J. H., and Madsen, M. S.: Surface Mass Balance of the Greenland Ice Sheet in the Regional Climate Model HIRHAM5: Present State and Future Prospects, p. 12, 2017.

Müller, W. A., Jungclaus, J. H., Mauritsen, T., Baehr, J., Bittner, M., Budich, R., Bunzel, F., Esch, M., Ghosh, R., Haak, H., Ilyina, T., Kleine, T., Kornblueh, L., Li, H., Modali, K., Notz, D., Pohlmann, H., Roeckner, E., Stemmler, I., Tian, F., and Marotzke, J.: A Higher-Resolution Version of the Max Planck Institute Earth System Model (MPI-ESM1.2-HR), Journal of Advances in Modeling Earth Systems, 0, https://doi.org/10.1029/2017MS001217, 2018.

Neale, R. B., Chen, C.-C., Gettelman, A., Lauritzen, P. H., Park, S., Williamson, D. L., Conley, A. J., Garcia, R., Kinnison, D., and Lamarque, J.-F.: Description of the NCAR Community Atmosphere Model (CAM 5.0), NCAR Tech. Note NCAR/TN-486+ STR, 2012.

Noël, B., van de Berg, W. J., van Meijgaard, E., Kuipers Munneke, P., van de Wal, R. S. W., and van den Broeke, M. R.: Evaluation of the Updated Regional Climate Model RACMO2.3: Summer Snowfall Impact on the Greenland Ice Sheet, The Cryosphere, 9, 1831–1844, https://doi.org/10.5194/tc-9-1831-2015, 2015.

Noël, B., van de Berg, W. J., Machguth, H., Lhermitte, S., Howat, I., Fettweis, X., and van den Broeke, M. R.: A Daily, 1 Km Resolution Data Set of Downscaled Greenland Ice Sheet Surface Mass Balance (1958–2015), The Cryosphere, 10, 2361–2377, https://doi.org/10.5194/tc-10-2361-2016, 2016.

Noël, B., van de Berg, W. J., van Wessem, J. M., van Meijgaard, E., van As, D., Lenaerts, J. T. M., Lhermitte, S., Kuipers Munneke, P., Smeets, C. J. P. P., van Ulft, L. H., van de Wal, R. S. W., and van den Broeke, M. R.: Modelling the Climate and Surface Mass Balance of Polar Ice Sheets Using RACMO2 – Part 1: Greenland (1958–2016), The Cryosphere, 12, 811–831, https://doi.org/10.5194/tc-12-811-2018, 2018.

Oleson, K. W.: Technical Description of Version 4.5 of the Community Land Model (CLM), NCAR Technical Note NCAR/TN-503+ STR, National Center for Atmospheric Research, Boulder, CO, 2013.

Picard, G., Domine, F., Krinner, G., Arnaud, L., and Lefebvre, E.: Inhibition of the Positive Snow-Albedo Feedback by Precipitation in Interior Antarctica, Nature Climate Change, 2, 795–798, https://doi.org/10.1038/nclimate1590, 2012.

Pollard, D.: A Retrospective Look at Coupled Ice Sheet–Climate Modeling, Climatic Change, 100, 173–194, https://doi.org/10.1007/s10584-010-9830-9, 2010.

Punge, H. J., Gallée, H., Kageyama, M., and Krinner, G.: Modelling Snow Accumulation on Greenland in Eemian, Glacial Inception, and Modern Climates in a GCM, Climate of the Past, 8, 1801– 1819, https://doi.org/10.5194/cp-8-1801-2012, 2012.

Rae, J. G. L., Aðalgeirsdóttir, G., Edwards, T. L., Fettweis, X., Gregory, J. M., Hewitt, H. T., Lowe, J. A., Lucas-Picher, b., Mottram, R. H., Payne, A. J., Ridley, J. K., Shannon, S. R., van de Berg, W. J., van de Wal, R. S. W., and van den Broeke, M. R.: Greenland Ice Sheet Surface Mass Balance: Evaluating Simulations and Making Projections with Regional Climate Models, The Cryosphere, 6, 1275–1294, https://doi.org/10.5194/tc-6-1275-2012, 2012.

Rhoades, A. M., Huang, X., Ullrich, P. A., and Zarzycki, C. M.: Characterizing Sierra Nevada Snowpack Using Variable-Resolution CESM, J. Appl. Meteor. Climatol., 55, 173–196, https://doi.org/10.1175/JAMC-D-15-0156.1, 2015.

Rhoades, A. M., Ullrich, P. A., and Zarzycki, C. M.: Projecting 21st Century Snowpack Trends in Western USA Mountains Using Variable-Resolution CESM, Clim Dyn, pp. 1–28, https://doi.org/10.1007/s00382-017-3606-0, 2017.

Rhoades, A. M., Ullrich, P. A., Zarzycki, C. M., Johansen, H., Margulis, S. A., Morrison, H., Xu, Z., and Collins, W.: Sensitivity of Mountain Hydroclimate Simulations in Variable-Resolution CESM to Microphysics and Horizontal Resolution, Journal of Advances in Modeling Earth Systems, https://doi.org/10.1029/2018MS001326, 2018.

Rignot, E. and Mouginot, J.: Ice Flow in Greenland for the International Polar Year 2008–2009, Geophysical Research Letters, 39, https://doi.org/10.1029/2012GL051634, 2012.

Small, R. J., Bacmeister, J., Bailey, D., Baker, A., Bishop, S., Bryan, F., Caron, J., Dennis, J., Gent, P., Hsu, H.-m., Jochum, M., Lawrence, D., Muñoz, E., diNezio, P., Scheitlin, T., Tomas, R., Tribbia, J., Tseng, Y.-h., and Vertenstein, M.: A New Synoptic Scale Resolving Global Climate Simulation Using the Community Earth System Model, Journal of Advances in Modeling Earth Systems, 6, 1065–1094, https://doi.org/10.1002/2014MS000363, 2014.

Sodemann, H., Schwierz, C., and Wernli, H.: Interannual Variability of Greenland Winter Precipitation Sources: Lagrangian Moisture Diagnostic and North Atlantic Oscillation Influence, Journal of Geophysical Research: Atmospheres, 113, https://doi.org/10.1029/2007JD008503, 2008.

Swenson, S. C. and Lawrence, D. M.: A New Fractional Snow-Covered Area Parameterization for the Community Land Model and Its Effect on the Surface Energy Balance, Journal of Geophysical Research: Atmospheres, 117, https://doi.org/10.1029/2012JD018178, 2012.

Ullrich, P. A.: SQuadGen: Spherical Quadrilateral Grid Generator, 2014.

van Angelen, J. H., M. Lenaerts, J. T., van den Broeke, M. R., Fettweis, X., and van Meijgaard, E.: Rapid Loss of Firn Pore Space Accelerates 21st Century Greenland Mass Loss, Geophys. Res. Lett., 40, 2109–2113, https://doi.org/10.1002/grl.50490, 2013.

van den Broeke, M. R., Enderlin, E. M., Howat, I. M., Kuipers Munneke, P., Noël, B. P. Y., van de Berg, W. J., van Meijgaard, E., and Wouters, B.: On the Recent Contribution of the Greenland Ice Sheet to Sea Level Change, The Cryosphere, 10, 1933–1946, https://doi.org/10.5194/tc-10-1933-2016, 2016.

van Kampenhout, L., Lenaerts, J. T. M., Lipscomb, W. H., Sacks, W. J., Lawrence, D. M., Slater, A. G., and van den Broeke, M. R.: Improving the Representation of Polar Snow and Firn in the Community Earth System Model, J. Adv. Model. Earth Syst., 9, 2583–2600, https://doi.org/10.1002/2017MS000988, 2017.

Van Tricht, K., Lhermitte, S., Lenaerts, J. T. M., Gorodetskaya, I. V., L'Ecuyer, T. S., Noël, B., van den Broeke, M. R., Turner, D. D., and van Lipzig, N. P. M.: Clouds Enhance Greenland Ice Sheet Meltwater Runoff, Nature Communications, 7, 10 266, https://doi.org/10.1038/ncomms10266, 2016.

Vizcaíno, M., Lipscomb, W. H., Sacks, W. J., van Angelen, J. H., Wouters, B., and van den Broeke, M. R.: Greenland Surface Mass Balance as Simulated by the Community Earth System Model. Part I: Model Evaluation and 1850–2005 Results, Journal of Climate, 26, 7793–7812, https://doi.org/10.1175/JCLI-D-12-00615.1, 2013.

Wehner, M. F., Reed, K. A., Li, F., Prabhat, Bacmeister, J., Chen, C.-T., Paciorek, C., Gleckler, P. J., Sperber, K. R., Collins, W. D., Gettelman, A., and Jablonowski, C.: The Effect of Horizontal Resolution on Simulation Quality in the Community Atmospheric Model, CAM5.1, J. Adv. Model. Earth Syst., 6, 980–997, https://doi.org/10.1002/2013MS000276, 2014.

Zarzycki, C. M. and Jablonowski, C.: A Multidecadal Simulation of Atlantic Tropical Cyclones Using a Variable-Resolution Global Atmospheric General Circulation Model, J. Adv. Model. Earth Syst., 6, 805–828, https://doi.org/10.1002/2014MS000352, 2014.

Zarzycki, C. M., Levy, M. N., Jablonowski, C., Overfelt, J. R., Taylor, M. A., and Ullrich, P. A.: Aquaplanet Experiments Using CAM's Variable-Resolution Dynamical Core, Journal of Climate, 27, 5481–5503, https://doi.org/10.1175/JCLI-D-14-00004.1, 2014.

Zarzycki, C. M., Jablonowski, C., Thatcher, D. R., and Taylor, M. A.: Effects of Localized Grid Refinement on the General Circulation and Climatology in the Community Atmosphere Model, J. Climate, 28, 2777–2803, https://doi.org/10.1175/JCLI-D-14-00599.1, 2015.

Ziemen, F., Rodehacke, C., and Mikolajewicz, U.: Coupled Ice Sheet–Climate Modeling under Glacial and Pre-Industrial Boundary Conditions, Climate of the Past, 10, 1817–1836, https://doi.org/10.5194/cp-10-1817-2014, 2014.